Conformational sampling of aminoacyl-tRNA during selection observed on single ribosomes

Peter Geggier[1], Richa Dave[1,2,#], Michael B. Feldman[1,3,#], Daniel S. Terry[1,4], Roger B. Altman[1], James B. Munro[1], Scott C. Blanchard[1]*

[1]*Department of Physiology and Biophysics, Weill Medical College of Cornell University, 1300 York Avenue, New York, NY 10065, USA*
[2]*Tri-Institutional Program in Chemical Biology, Weill-Cornell Medical College of Cornell University,*
[3]*Weill Cornell / Rockefeller University / Sloan-Kettering Tri-Institutional MD-PhD Program,*
[4]*Tri-Institutional Training Program in Computational Biology and Medicine*
[#]*These authors contributed equally to this work*

SUPPLEMENTAL MATERIAL

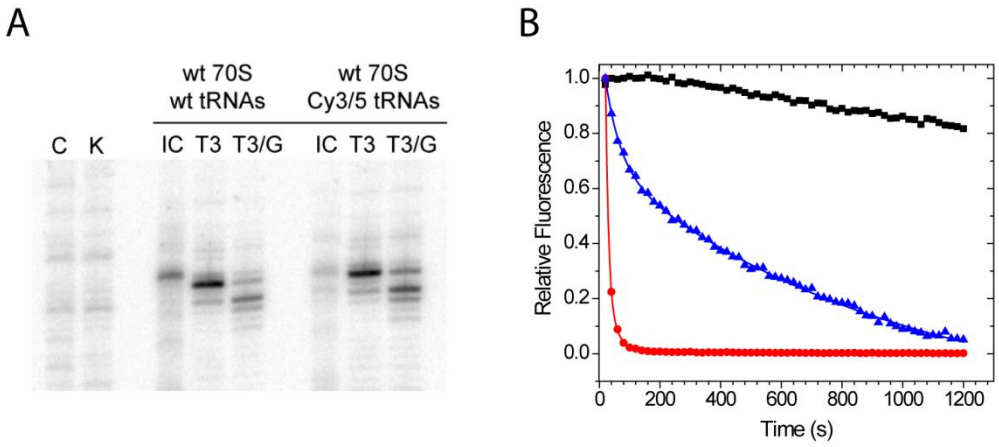

Supplemental Figure 1: Ribosome complexes are competent in tRNA selection and translocation. (**A**) Toeprinting assays indicate that fluorescently labeled tRNAs are fully competent in the extent of A-site tRNA accommodation and translocation. IC lanes: Initiation complexes containing fMet-tRNA^{fMet} in the P site. T3 lanes: Pre-translocation ribosome complexes bearing deacylated P-site tRNA^{fMet} and fMet-Phe-tRNA^{Phe} in the A site. T3/G lanes: After incubation with 10μM EF-G and 2mM GTP for 2 minutes at room temperature. For "Cy3/5 tRNAs" experiments, site-specifically labeled A- and P-site tRNAs, tRNA^{Phe}(acp^{3}U47), tRNA^{fMet}(Cy3-s^{4}U8), respectively were used. C lane: dideoxycytidine sequencing lane. K lane: unmodified rRNA control. (**B**) Fluorescence-based puromycin (Pmn) reactivity assay [1]. The rate of Pmn reactivity reports on A-site PTC occupancy. In the absence of Pmn, surface-immobilized ribosome complexes carrying Cy3-Met-tRNA^{fMet} in the P-site show negligible loss in fluorescence due to photobleaching and dissociation over the observation window (black squares). These complexes readily react with Pmn, resulting in loss of surface localized fluorescence due to dissociation of the Cy3-Met-Pmn moiety (red circles). Following enzymatic delivery of unlabeled Phe-tRNA^{Phe} to surface-immobilized ribosome complexes, resulting in transfer of the fluorescently labeled peptide to the A site tRNA, Pmn reactivity is substantially attenuated (blue triangles). Residual Pmn reactivity results from transient excursions to the Pmn-reactive A/P hybrid state[1; 2].

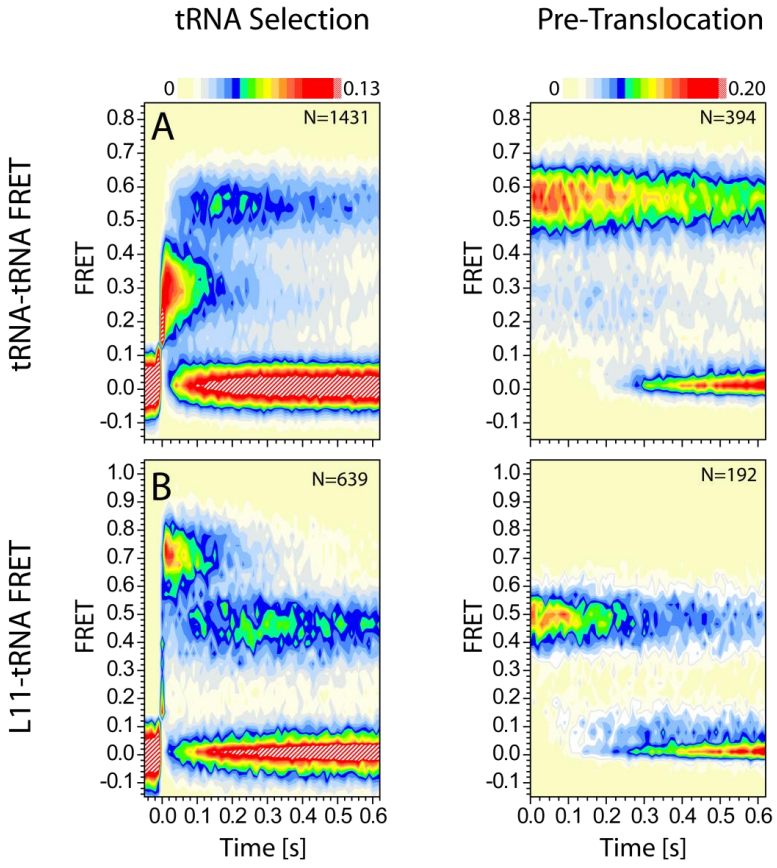

Supplemental Figure 2: The AC state corresponds to the classical tRNA configuration. (A) Population FRET histograms generated upon stop-flow delivery of $tRNA^{Phe}$(Cy5-acp^3U47) ternary complex to ribosome complexes containing P-site $tRNA^{fMet}$(Cy3-s^4U8) (left panel) and following a one minute incubation period (right panel). (B) Population FRET histograms generated upon stop-flow delivery of $tRNA^{Phe}$(Cy5-acp^3U47) ternary complex to ribosome complexes containing (Cy3-C39)-labeled L11 (left panel) and following a one minute incubation period (right panel).

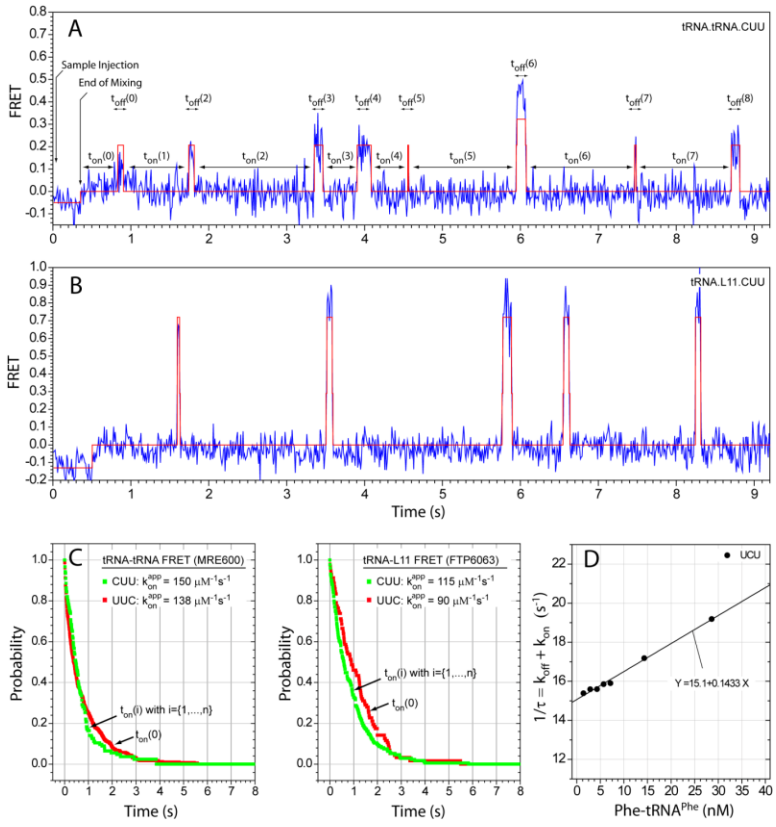

Supplemental Figure 3: Cognate and near-cognate tRNA arrive at the codon-recognition (CR) state in a codon-independent fashion according to the known bimolecular rate constant for the ternary complex-ribosome interaction. (A) An example smFRET trajectory (blue) observed upon delivery of 10nM Phe-tRNA^{Phe}(Cy5-acp^{3}U47) ternary complex to surface-immobilized ribosome complexes bearing deacylated tRNA^{fMet}(Cy3-s^{4}U8) in the P-site and programmed with a near-cognate CUU codon in the A site. (B) an example smFRET trajectory (blue) observed upon delivery of 10nM Phe-tRNA^{Phe}(Cy5-acp^{3}U47) ternary complex to surface-immobilized ribosome complexes bearing a donor-labeled L11 protein and programmed with a near-cognate CUU codon in the A site. Here, repeated binding-unbinding events were identified by short-lived dwells in non-zero FRET states above a FRET threshold of ≥0.13. For both systems, dwell times in zero- and non-zero FRET states were identified through idealization (red) to the model shown in **Supplemental Figure 6C**. (C) The lifetimes in zero (t_{on}) and non-zero FRET states (t_{off}) were determined by compiling the dwell times in zero FRET (t_{on}) into survival plots. Data obtained from both P-site tRNA (left panel) and L11-labeled (center panel) complexes were fit to a double exponential function of the form: $\boldsymbol{y = A_1 e^{-x/t1} + A_2 e^{-x/t2}}$. The lifetimes were calculated according to the weighted average of both fast and slow components of the decay. The bimolecular rate constants for ternary complex binding to both P-site tRNA- and L11-labeled ribosome complexes programmed with cognate (UUC) and near-cognate (CUU) A-site codons were estimated from the calculated lifetimes of the zero-FRET states after adjusting for the ternary complex concentration ([T3]) (D) The concentration dependence of the initial binding reaction was determined for the complex bearing Cy3-labeled tRNA^{fMet} in the P site with UCU codon by measuring the relaxation time, τ, as a

function of ternary complex concentration [T3] and fitting the data to the equation: $\boldsymbol{1/\tau = k_{off}^{app} + k_{on}^{app} \cdot [T3]}$. Here, the bimolecular rate constant is represented by the slope of the fitted line (143 μM^{-1} s^{-1}) and the apparent dissociation rate, from the aggregate of non-zero FRET states is given by the line's intersection with the vertical axis ($15 s^{-1}$). Similar findings were observed for both cognate- and near-cognate (CUU)- programmed ribosomes. However, these data are not shown as they have higher uncertainties owing to missed event considerations in the case of CUU complexes and the limited data set that could be obtained in the case of the cognate system because of the relatively high incorporation efficiency of this system.

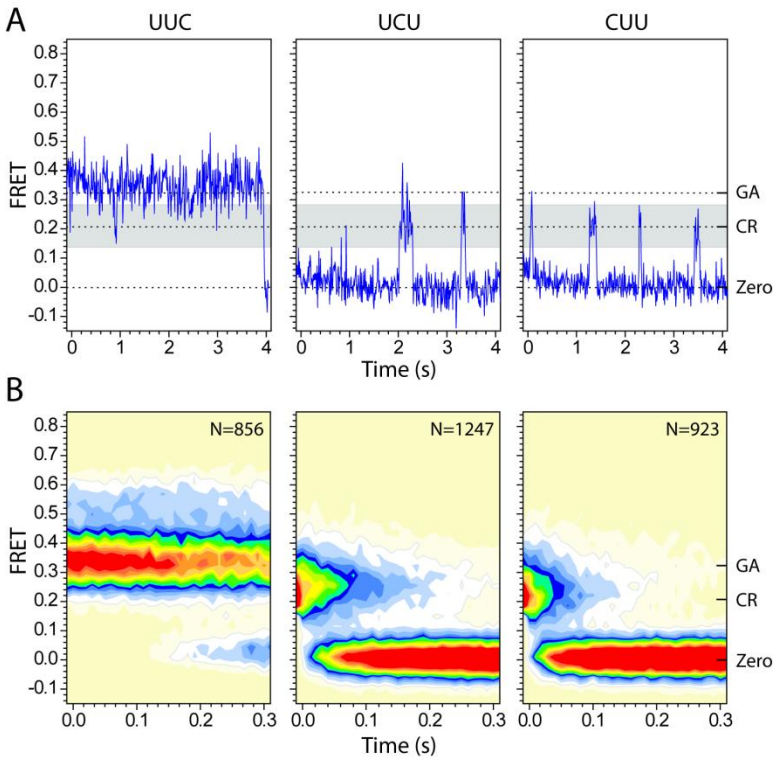

Supplemental Figure 4: The FRET states observed for GDPNP-stalled aa-tRNA selection events are different for cognate and near-cognate complexes. (A) smFRET FRET trajectories (blue) observed after a one minute incubation of 10 nM Phe-tRNA^{Phe}(Cy5-acp^{3}U47) ternary complex in the presence of 100 µM GDPNP to cognate (UUC-left panel) and near-cognate (UCU-center panel; and CUU-right panel) programmed, surface-immobilized ribosome complexes bearing deacylated tRNA^{fMet}(Cy3-s^{4}U8) in the P-site. Experiments were performed in Tris-Polymix buffer at 15mM Mg^{2+}. For reference the mean FRET value (dotted line) and the standard deviation (blue shaded area) of the low-FRET, codon-recognition (CR) state are shown. (B) Corresponding FRET histograms for cognate (UUC-left panel) and near-cognate (UCU-center panel; and CUU-right panel) programmed ribosome complexes. On average the FRET maxima of the dominant state for the three complexes are: $FRET_{max}$(UUC) = 0.33, $FRET_{max}$(UCU) = 0.25 and $FRET_{max}$(CUU) = 0.23.

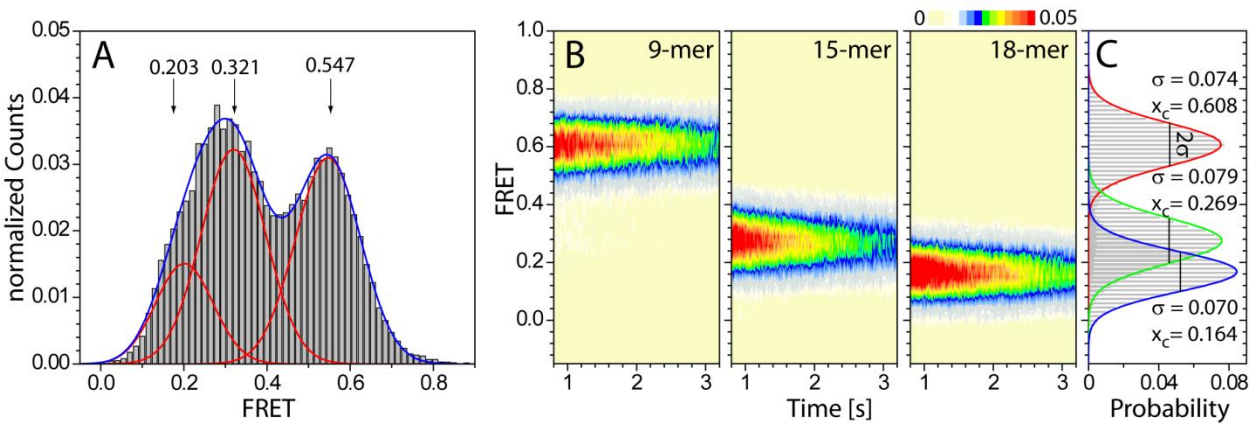

Supplemental Figure 5: Curve fitting of a three-state FRET-histogram. (A) Population FRET histograms of the raw data obtained upon delivery of 10 nM Phe-tRNA^{Phe}(Cy5-acp^{3}U47) ternary complex to surface-immobilized ribosome complexes bearing deacylated tRNA^{fMet}(Cy3-s^{4}U8) in the P-site programmed to contain a cognate UUC codon in the A site. Here, data were fit to the sum of multiple Gaussians where the standard deviation of each state was constrained to the window, $0.069 \leq \sigma \leq 0.079$. In so doing, three Gaussian distributions were shown to adequately describe the data where $x_{c1} = 0.203$, $x_{c2} = 0.321$ and $x_{c3} = 0.547$. (B) Cy3- and Cy5-labeled DNA oligonucleotides containing 9, 15, or 18 base pairs were surface-immobilized for smFRET imaging, as previously described[3] and imaged under the identical conditions of the selection experiment. These data yield population FRET histograms whose observed width provides the standard deviation in FRET values observed for conformationally-rigid structures and therefore a well-defined FRET state. (C) Histograms compiled for each of these data sets were fit to Gaussian distributions, where x_c is the mean FRET value and σ is the standard deviation of that FRET state. From these three independent fits a mean standard deviation $\langle\sigma\rangle$ of 0.074 ± 0.005 was estimated.

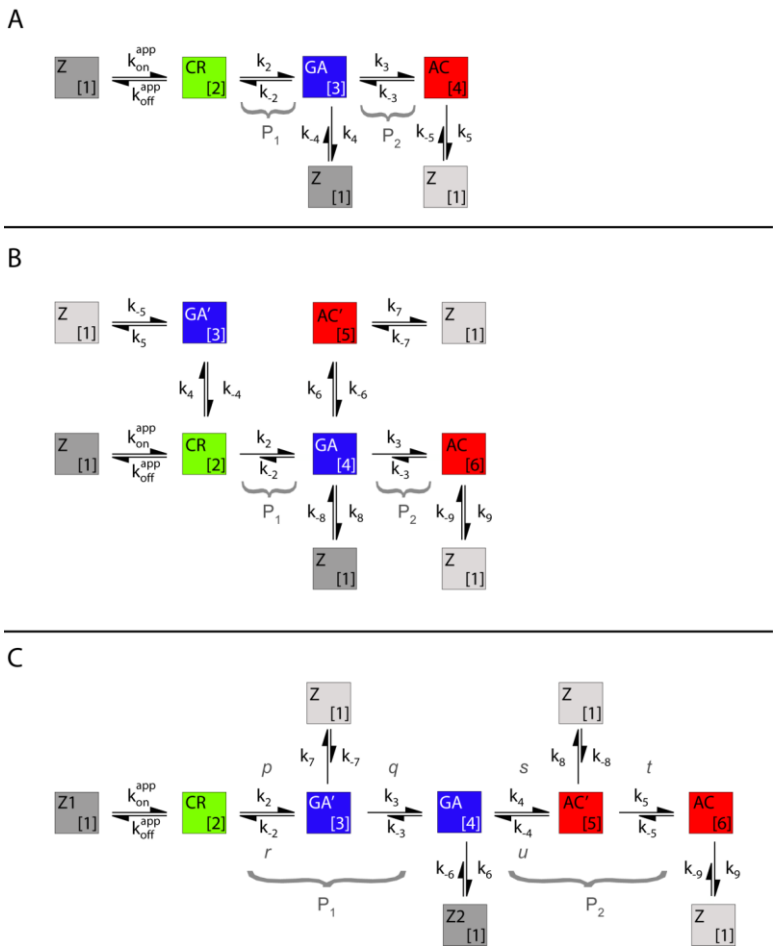

Supplemental Figure 6: Kinetic models of tRNA selection. Individual FRET events were extracted from movies of the selection process and subjected to quantitative analyses using automated hidden Markov Modeling (HMM) procedures. Individual FRET events were idealized using a segmental k-means (SKM) algorithm in QuB to fully-reversible, kinetic models of increasing complexity, where each non-zero FRET state in the model was also connected to a zero-FRET state to account for the theoretically non-zero probability of photobleaching and/or dissociation from each state. Each model consists of three distinct states corresponding to the experimentally observed CR, GA and AC configurations: 0.21, 0.32, 0.54 FRET (averaged FRET values obtained from the fitting of three different population FRET histograms) for P-site tRNA-labeled complexes; 0.73, 0.73, and 0.46 for L11-labeled complexes. In each case the standard deviation, σ, was defined according to the value obtained for DNA oligonucleotide control samples (σ = 0.074 ± 0.005; **Supplemental Figure 5**). (A) The minimal four states model. (B) A branched model geometry similar to that proposed previously[4], in which off-pathway FRET states of similar FRET values to their connection points may be sampled. (C) A linear geometry containing redundant states of similar FRET value, where each is on path to the fully accommodated (AC) state. Model A was unable to adequately describe the smFRET data, where transitions between FRET states were generally observed to occur on two distinct time scales[4]. Models B and C, which both contain reversible selection steps that allow for distinct transition time scales, enable the calculation of transition probabilities (P_1 and P_2) between FRET states. In Model B, the transition probabilities, P_1 and P_2 are dependent only on the

forward rates, k_2, k_3 and k_4, k_6; off-pathway rates from transiently sampled states, k_{-4} and k_{-6}, do not contribute to the calculation. In Model C, the transient states are on pathway, and therefore both forward (k_2, k_4) and reverse sampling rates (k_{-2}, k_{-4}) also contribute to the transition probability calculation (**Supplemental Table 1**). This linear reaction model, consisting of reversible steps, preceding essentially irreversible chemistry steps, is reminiscent of the kinetic proofreading model originally proposed by Hopfield[5]. This reaction pathway, by virtue of its ability to fit both the experimental observations and previously established models of aa-tRNA selection, was therefore used to idealize all systems investigated and to perform simulations. Here, transient GA' and AC' FRET states were assigned to values and standard deviations identical to those given to GA and AC states in their respective systems. For idealization using a segmental k-means (SKM) algorithm[6], the initial parameters were set to a value five-times slower than our time resolution ($k_i = 20s^{-1}$) with the exception that the experimentally-determined bimolecular rate constant were used ($k_{on}^{app} = 1.4s^{-1}$ at 10nM ternary complex concentration) (**Supplemental Figure 3**). Solely for the purpose of idealization, backwards rates from irreversible steps (k_{-3}, k_{-5}) were set to be $0.2s^{-1}$.

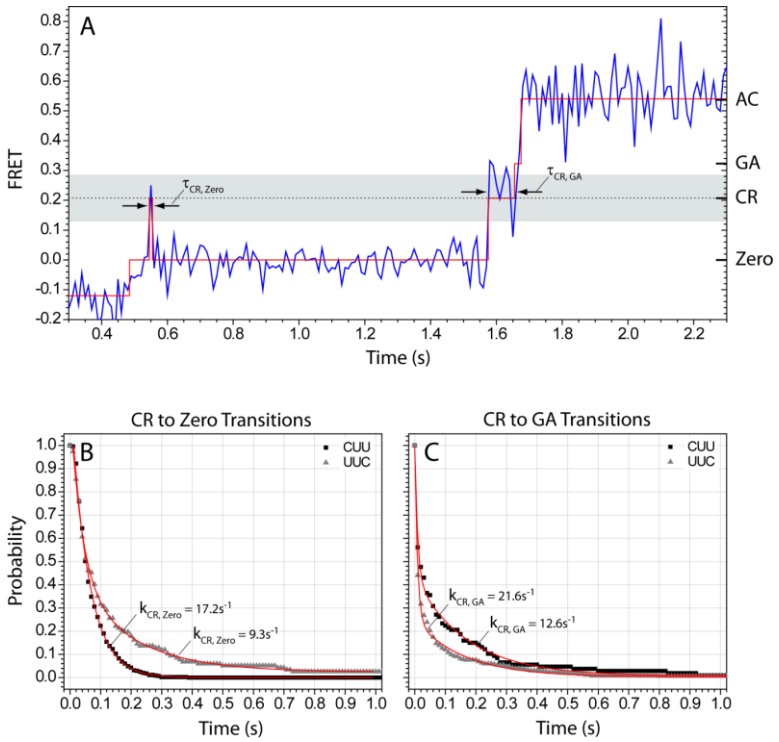

Supplemental Figure 7: The lifetime of the low-FRET state is codon dependent and is thus defined as the codon-recognition (CR) state. (A) A representative smFRET FRET trajectory (blue) observed following stop flow delivery of 10 nM Phe-tRNA^{Phe}(Cy5-acp^{3}U47) ternary complex to the UUC (cognate)-programmed, surface-immobilized ribosome complexes. Idealization of these data (red) was performed according to the kinetic model shown in **Supplemental Figure 6C**. The time course of the trace shows that the ternary complex samples a low-FRET state and then returns to zero FRET prior to later binding events that lead to complete accommodation into the A site of the ribosome. For reference the mean FRET value (dotted line) and the standard deviation (shaded area) of the low-FRET state are shown. (B) Differences in the lifetimes of low-FRET state events that immediately return to zero FRET ($\tau_{CR, Zero}$) are observed for cognate and near-cognate complexes, demonstrating codon dependence. (C) As expected for the codon-recognition state (CR), the lifetime of the low-FRET state was also observed to be codon dependent for transitions to higher-FRET states ($\tau_{CR, GA}$). As anticipated for an induced-fit model of aa-tRNA selection, $\tau_{CR, GA}$ is shorter for complexes programmed with a cognate codon. With the exception of the CUU lifetimes $\tau_{CR, Zero}$, which follow a single exponential distribution, all data were fit to a double exponential decay function. From this analysis the following weighted-average decay rates were estimated: $k_{CR, Zero}$ (CUU) = 17.2s^{-1}, $k_{CR, Zero}$ (UUC)= 9.3 s^{-1}, $k_{CR,GA}$ (CUU) = 12.6 s^{-1} and $k_{CR,GA}$ (UUC) = 21.6 s^{-1}.

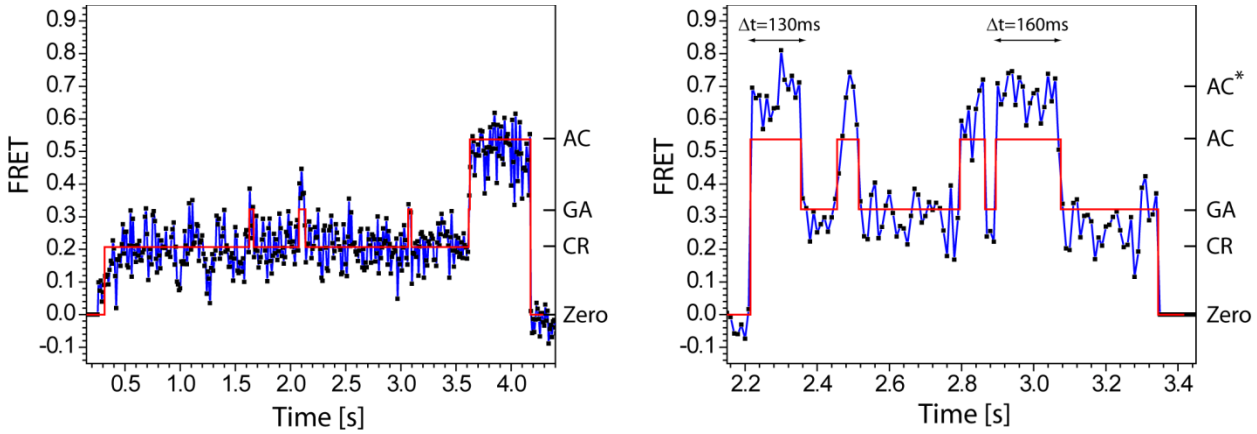

Supplemental Figure 8: The majority of FRET events quantitatively designated as "productive" binding events for complexes programmed with a near-cognate mRNA exhibit unusual kinetic and FRET characteristics followed by dissociation from the ribosome. smFRET trajectories (blue) obtained from delivery of 10 nM Phe-tRNA^{Phe}(Cy5-acp^{3}U47) ternary complex to surface-immobilized ribosome complexes bearing deacylated tRNA^{fMet}(Cy3-s^{4}U8) in the P-site programmed to contain a near-cognate CUU codon in the A site. Experiments were performed in Tris-Polymix buffer at 15mM Mg^{2+}. Data were idealized (red) according to the kinetic model shown in **Supplemental Figure 6C**. (Left panel) An example smFRET trajectory showing an unusually long delay during initial selection (transitioning between CR and GA'/GA states prior to a relatively short-lived excursion to an AC-like dwell lasting ~400ms followed be either dissociation or photobleaching. (Right panel) An example smFRET trajectory showing repeated excursion into AC* states, characterized by a FRET value substantially higher than that assigned to the AC state (~0.54). In both cases, the lifetimes in AC-like states surpass the established criterion for classification as a productive binding event (an AC state dwell lasting ≥120ms), but lack the characteristics of *bona fide* productive binding events –generally long-lived AC state dwells punctuated by transient excursions to hybrid states.

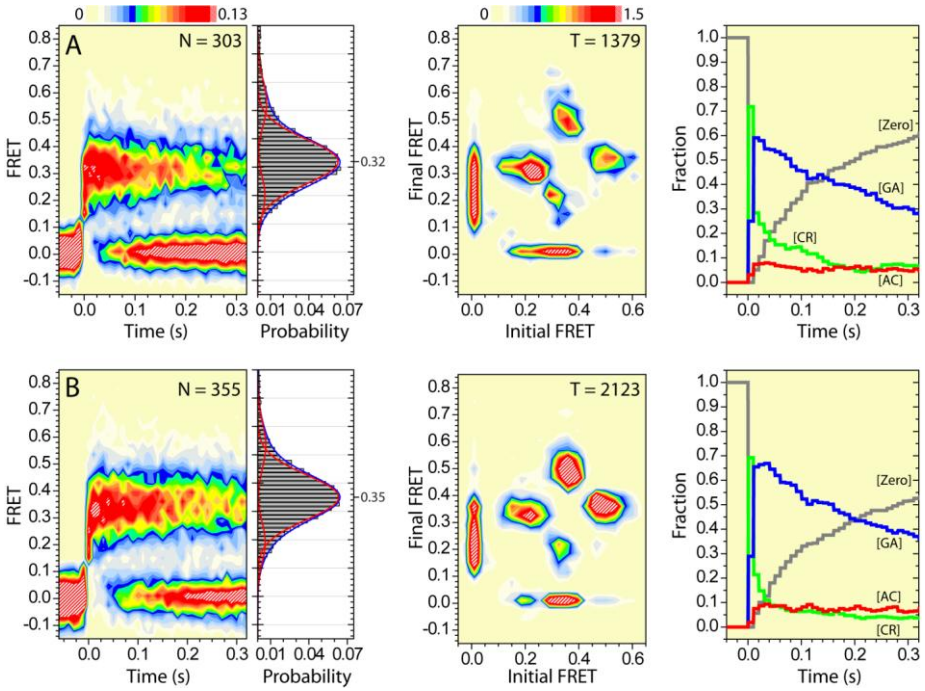

Supplemental Figure 9: Conformational sampling occurs before and after GTP-hydrolysis. Population FRET histograms and TDPs obtained from experiments in which 10 nM Phe-tRNA^{Phe}(Cy5-acp^{3}U47) ternary complex was delivered to surface-immobilized ribosome complexes bearing deacylated tRNA^{fMet}(Cy3-s^{4}U8) in the P-site and programmed with a cognate UUC codon in the A site in the presence of (A) 100µM non-hydrolyzable GTP analog, GDPNP, or (B) 20µM kirromycin. Both experiments were performed in Tris-Polymix buffer at 15 mM Mg^{2+}. The tRNA dissociates with a rate of 2.8s^{-1} from the GDPNP stalled complex and is slightly faster than the dissociation rate from the Kirromycin stalled complex (2.0s^{-1}).

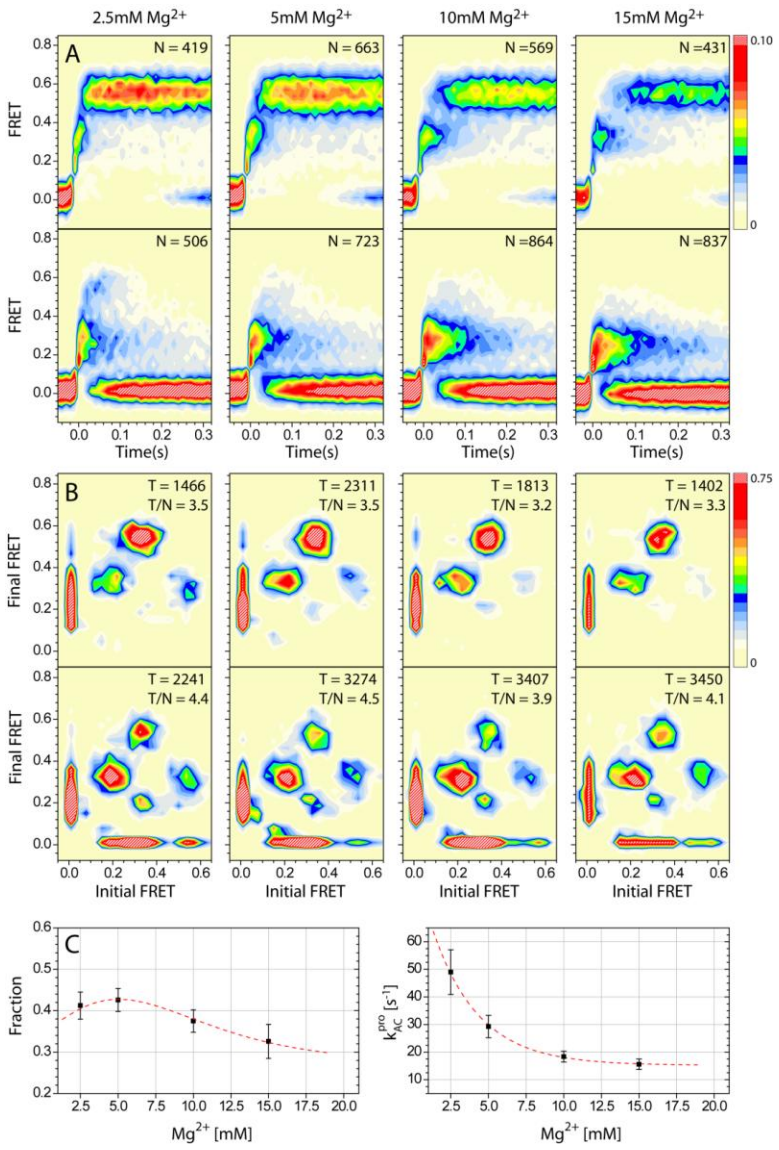

Supplemental Figure 10: The rate and efficiency of aa-tRNA selection is Mg^{2+} dependent. (A) Population FRET histograms and (B) TDPs for (upper panel) productive and (lower panel) non-productive selection events obtained from experiments in which 10 nM Phe-$tRNA^{Phe}$(Cy5-acp^{3}U47) ternary complex was delivered to surface-immobilized ribosome complexes bearing deacylated $tRNA^{fMet}$(Cy3-s^{4}U8) in the P-site programmed to contain a cognate UUC codon in the A site over a range of Mg^{2+} concentrations (2.5-15 mM). The total number of events in each class (N) and the number of transitions per trace (T/N) in each case are shown. From these data, the fraction of productive aa-tRNA accommodation events as a function of Mg^{2+} concentration (C, left panel) and the rate of forming the stable AC state formation as a function of Mg^{2+} concentration (C, right panel) were derived. While the rate of AC state formation increases 3-fold at lower Mg^{2+}, the T/N remains unchanged or increases. These data are indicative of increased rates of aa-tRNA dynamics in the A site at lower Mg^{2+} concentrations.

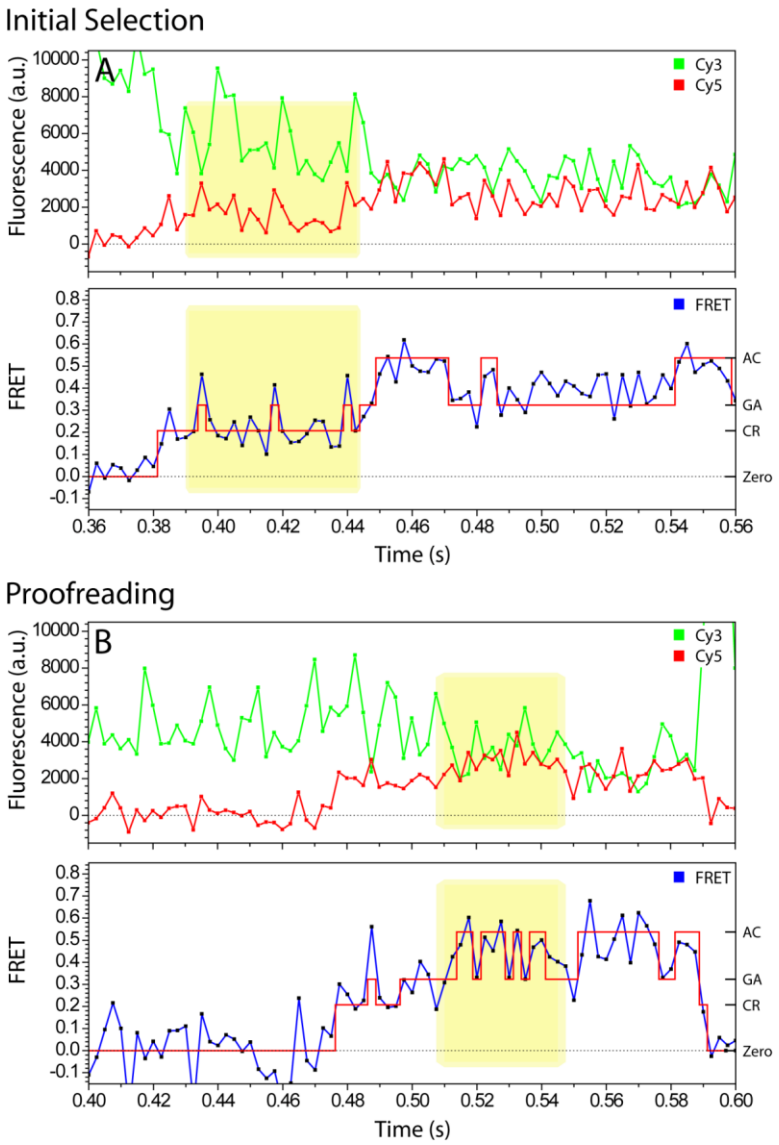

Supplemental Figure 11: Evidence of aa-tRNA motions in the A site occurring at rates ≥100-200s^{-1}. Representative single-molecule fluorescence and FRET trajectories obtained at 2.5 ms time resolution at 5mM Mg^{2+} showing single-data-point, anti-correlated fluctuations in Cy3 (green) and Cy5 (red) intensity. The existence of such fast dynamics supports the notion that cognate tRNA moves rapidly between CR and GA'/GA states during (A) initial selection and GA and AC'/AC states during (B) proofreading. FRET (blue) was idealized (red) according to the kinetic model shown in **Supplemental Figure 6C**. Regions corresponding to initial selection and proofreading are highlighted in yellow.

Step	Transition probabilities forward	Transition probabilities backward	Overall transition probabilities
INITIAL SELECTION			
GTPase activation; rate limited by tRNA motions	$p = \frac{k_2}{k_2 + k_{off}^{app}}$	$r = \frac{k_{-2}}{k_{-2} + k_7 + k_3}$	$P_1 = \frac{p \cdot q}{1 - p \cdot r}$
GTP hydrolysis	$q = \frac{k_3}{k_3 + k_{-2} + k_7}$		
PROOFREADING			
Accommodation; rate limited by tRNA motions	$s = \frac{k_4}{k_4 + k_6}$	$u = \frac{k_{-4}}{k_{-4} + k_8 + k_5}$	$P_2 = \frac{s \cdot t}{1 - s \cdot u}$
Peptide bond formation	$t = \frac{k_5}{k_5 + k_{-4} + k_8}$		
EFFICIENCY OF PRODUCT FORMATION			$P = P_1 \cdot P_2$

Supplemental Table 1: Calculation of Transition Probabilities. The model shown in **Supplemental Fig. 6C** predicts two selection steps with transition probabilities P_1 and P_2. A single selection step has an overall transition probability $P_i = x \cdot y/(1 - x \cdot z)$[Ref.7] with transition probabilities x=p, y=q, z=r for initial selection and x=s, y=t, z=u for proofreading.

STEP		Rate Constants in s^{-1} Cognate 15mM Mg^{2+}	Rate Constants in s^{-1} Near-Cognate 15mM Mg^{2+}
SUBSTRATE BINDING	k_{on}^{app} [1]	140	140
	k_{off}^{app}	14	20
INITIAL SELECTION			
Reversible tRNA motions (GTPase activation)	k_2	260	173
	k_{-2}	200	600
GTP hydrolysis	k_3	12	4
	k_{-3}	0	0
Transition probability $P_1(CR \rightarrow GA)$ [2]	**P_1**	**0.51**	**0.05**
PROOFREADING			
Reversible tRNA motions (accommodation)	k_4	90	50
	k_{-4}	30	76
Peptide bond formation	k_5	12	1
	k_{-5}	0	0
Transition probability $P_2(GA \rightarrow AC)$ [2]	**P_2**	**0.59**	**0.13**
DISSOCIATION PATHWAYS			
Rejection after GTP-Hydrolysis (GA)	k_6	9	2
	k_{-6}	0	0
Rejection before GTP-Hydrolysis (GA')	k_7	0	0
	k_{-7}	0	0
Rejection after GTP-Hydrolysis (AC')	k_8	4	4
	k_{-8}	0	0
Photo bleaching	k_9	2	2
OVERALL TRANSITION PROBABILITY: $P = P_1 \cdot P_2$	**P**	**0.30**	**0.007**

[1] k_{on}^{app} = bimolecular rate of enzyme and substrate binding in μM^{-1} s^{-1} (this rate is derived from experimental measurements of the arrival time at 10nM ternary complex concentration (**Supplemental Figure 3**).

[2] For the calculation of P_1 and P_2 see **Supplemental Table 1**

Supplemental Table 2: Elemental rate constants for tRNA selection. Shown here are the rates obtained from simulation and calculated transition probabilities (P_1, P_2) corresponding to the kinetic scheme shown in Supplemental Fig. 6C for the cognate and near-cognate aa-tRNA selection process on ribosome complexes bearing deacylated $tRNA^{fMet}$(Cy3-s^4U8) in the P-site. The simulation was carried out under the assumption that tRNA dissociates from the ribosome during the proofreading step directly after GTP-hydrolysis. As discussed in the text, the observed transition probability P into the AC state for near-cognate complexes (0.007) does not accurately report on the actual number of fully accommodated molecules. The majority of AC state observations passing the selection criteria (AC state lifetime $\geq$ 120ms) ultimately dissociate from the ribosome (Supplemental Figure 8). Thus, the actual probability of productive events is estimated to be much lower, on the order of ~0.001.

		smFRET		Bulk Measurements	
		Cognate	Near-Cognate	Cognate	Near-Cognate
k_{on}, k_1	($\mu M^{-1} s^{-1}$)	140	150	110[1], 60-80[3]	110[2], 60-80[3]
k_{cat}/Km	($\mu M^{-1} s^{-1}$)	72	7.5	88[2]	82[2]
F_p		0.59	0.13	≈ 1[2]	0.015[2]
f		10		1.07[2], 2[3]	
F		5		67[2], 10[3]	
S=*f*·F		50		72[2], 20[3]	

Supplemental Table 3: Comparison of estimated accuracy parameters obtained from smFRET measurements with literature values. All rates and fidelity parameters are estimated in the presence of high Mg^{2+} (>10 mM). k_{on}: Second-order association rate constant for substrate binding in the smFRET measurements (**Supplemental Figure 3, 6C**); k_1: Rate of initial binding (Gromadski *et. al.*[8]); k_{cat}/Km: For the smFRET measurements the parameter was calculated for the initial selection step according to the equation $k_{cat}/Km = k_{on} \cdot P_1^{Ref.9}$ (**Supplemental Table 1, 2**); F_p: Probability of incorporation during proofreading (P_2 in **Supplemental Table 1, 2**); *f*: Efficiency of initial selection. For the smFRET data this parameter was calculated according to the equation $f = P_1^{UUC} / P_1^{CUU}$ (**Supplemental Table 2**); F: Efficiency of proofreading. This parameter is given for the smFRET data through the equation $F = P_2^{UUC}/P_2^{CUU}$ (**Supplemental Table 2**); S: Overall Selectivity.

[1] UUU, 10mM Mg^{2+}, $PhetRNA^{Phe}$, Pape *et al.*[10]
[2] UUU, 10mM Mg^{2+}, $PhetRNA^{Phe}$, Pape *et al.*[11]
[3] UUC, CUU 20mM Mg^{2+}, $PhetRNA^{Phe}$, no polyamines, Gromadski *et al.*[8]

Supplemental Methods:

Simulation of smFRET-data

To test the proposed kinetic model (**Supplemental Fig. 6C**) smFRET trajectories were simulated at 100μs time resolution for the cases of both cognate and near-cognate A-site codons. In order to generate a complete set of rate constants for the model, an iterative fitting algorithm was used. The algorithm started with an initial set of rate constants estimated in part through global fitting of the dwell-time histogram data and from published values in the literature[12]. As the chemical steps of GTP-hydrolysis and peptide bond formation are generally considered irreversible, the two back reactions (GA→GA' and AC→AC') were constrained to a rate of zero. The rate of initial binding k_{on}^{app} was given through arrival time analysis (**Supplemental Table 2**) and was also held constant. All other rate constants were than refined by iterative variation. FRET traces simulated at 100μs time resolution were rebinned to 10ms so that the simulated FRET traces could be directly compared to the experimental data (**Figure 6**). In order to quantify the convergence of the solution, population FRET histograms, dwell-time histograms and TDPs, were generated from the simulated traces and directly compared to the experimental data (**Figure 6A**, right panels). Residuals were calculated by determining the difference between the experimental and simulated data. To a first approximation, this algorithm achieved approximate convergence, leading to the set of rate constants reported in **Supplemental Table 2.** These values represent the weighted-average behaviors of all the molecules in the system.

Preparation of L11-labeled ribosome complexes:

The L11 protein was isolated from BL21(DE3) cells harboring an expression vector encoding N-terminally SUMO-tagged L11 (Invitrogen). Purification was performed by Ni-NTA affinity chromatography (Quiagen), and site-specifically labeled at the native C39 by incubation for 1hr on ice with 1mM Cy3-maleimide (GE Healthcare, Piscataway, NJ) in a buffer containing 20mM MES pH6, 200mM KCl, 0.2mM TCEP. Excess dye was separated from the protein through a second round of Ni-NTA chromatography. The sumo-tagged, Cy3-labeled L11 protein was purified by Mono-S, cation-exchange chromatography (GE Healthcare) under denaturing conditions (6M urea) using a linear gradient of 0-100 1M KCl buffered to pH=6.The SUMO tag was removed by proteolytic digestion. Ribosomes were isolated from an L11-knockout strain carrying a wild-type plasmid-encoded L11 gene (a kind gift from Dr. Suparna Sanyal) after passive curing the strain of the L11-plasmid. Purified, native L11(Cy3-C39) was reconstituted with ribosomes isolated from the ΔL11 knock-out strain through incubation with two-fold excess labeled protein according to published procedures[13]. Initiation complexes were then prepared with unlabeled $tRNA^{fMet}$ as described for MRE600 ribosomes (**Methods**).

Estimation of bulk translation rates at physiological magnesium ion concentrations.

To estimate the rate of cognate aa-tRNA selection in presence of near-cognate aa-tRNAs, consideration was given to both to the estimated transit time for productive cognate selection as well as the time for rejection of all non-productive selection events obtained from the analysis of selection at 2.5mM Mg^{2+}. Here, the efficiency of productive cognate selection was estimated to be ~45% and the rate of productive cognate selection events was estimated at ~$48s^{-1}$. Thus, in the absence of competition for the A site from near-cognate tRNAs, the average rate of pre-translocation complex formation at 2.5mM Mg^{2+} and at 20°C can be estimated at ~$21s^{-1}$ ($0.45 \cdot 48s^{-1}$), an effective transit time of ~48ms. However the actual rate of selection must take into consideration that: 1] near-cognate tRNAs have the same apparent bimolecular rate constant for the A site (**Supplemental Figure 3**); 2] there are ~50

distinct tRNA genes in *E.coli*[14] of which only 1-4 may be cognate to the mRNA codon and; 3] the estimated dissociation rate for non-productive cognate and near-cognate tRNA binding events are ~50ms and ~5ms, respectively. Thus, assuming near saturating concentrations of ternary complex in the cell[9] and equivalent tRNA expression levels there will be ~20 near- and non-cognate tRNA binding events on average, each lasting ~5ms, prior to a cognate tRNA binding event. This amounts to a dead time of ~100ms between cognate selection events. Thus, assuming that the ribosome spends ~4% of the time unbound under rapid growth conditions[9; 14], the observed rate of protein synthesis can be estimated from these values to be ~$4.8s^{-1} \cong 0.96$ / (0.048s + 0.050s + 0.100s). A similar analysis at 15mM Mg^{2+} suggests substantially slower translation. Following the same assumptions, bulk translation rates would be $0.5s^{-1} \cong 0.96$ / (0.202s+0.070s+1.600s).

REFERENCES:

1. Blanchard, S. C., Kim, H. D., Gonzalez, R. L., Jr., Puglisi, J. D. & Chu, S. (2004). tRNA dynamics on the ribosome during translation. *Proc Natl Acad Sci USA* **101**, 12893-8.
2. Sharma, D., Southworth, D. R. & Green, R. (2004). EF-G-independent reactivity of a pre-translocation-state ribosome complex with the aminoacyl tRNA substrate puromycin supports an intermediate (hybrid) state of tRNA binding. *RNA* **10**, 102-13.
3. Dave, R., Terry, D. S., Munro, J. B. & Blanchard, S. C. (2009). Mitigating Unwanted Photophysical Processes for Improved Single-Molecule Fluorescence Imaging. *Biophys J* **96**, 2371-2381.
4. Lee, T.-H., Blanchard, S. C., Kim, H. D., Puglisi, J. D. & Chu, S. (2007). The role of fluctuations in tRNA selection by the ribosome. *Proceedings of the National Academy of Sciences* **104**, 13661-13665.
5. Hopfield, J. J. (1974). Kinetic proofreading:a new mechanism for reducing errors in biosynthetic processes requiring high specificity. *Proc. Natl. Acad. Sci.* **71**, 4135-4139.
6. Qin, F. (2004). Restoration of single-channel currents using the segmental k-means method based on hidden Markov modeling. *Biophys J* **86**, 1488-501.
7. Ninio, J. (1975). Kinetic amplification of enzyme discrimination. *Biochimie* **57**, 587-595.
8. Gromadski, K. B., Daviter, T. & Rodnina, M. V. (2006). A uniform response to mismatches in codon-anticodon complexes ensures ribosomal fidelity. *Mol Cell* **21**, 369-77.
9. Johansson, M., Lovmar, M. & Ehrenberg, M. (2008). Rate and accuracy of bacterial protein synthesis revisited. *Curr Opin Microbiol* **11**, 141-7.
10. Pape, T., Wintermeyer, W. & Rodnina, M. V. (1998). Complete kinetic mechanism of elongation factor Tu-dependent binding of aminoacyl-tRNA to the A site of the E-coli ribosome. *Embo Journal* **17**, 7490-7497.
11. Pape, T., Wintermeyer, W. & Rodnina, M. (1999). Induced fit in initial selection and proofreading of aminoacyl-tRNA on the ribosome. *Embo Journal* **18**, 3800-3807.
12. Rodnina, M. V., Gromadski, K. B., Kothe, U. & Wieden, H. J. (2005). Recognition and selection of tRNA in translation. *FEBS Lett* **579**, 938-42.
13. Wang, Y., Qin, H., Kudaravalli, R. D., Kirillov, S. V., Dempsey, G. T., Pan, D., Cooperman, B. S. & Goldman, Y. E. (2007). Single-molecule structural dynamics of EF-G--ribosome interaction during translocation. *Biochemistry* **46**, 10767-75.
14. Lovmar, M. & Ehrenberg, M. (2006). Rate, accuracy and cost of ribosomes in bacterial cells. *Biochimie* **88**, 951-61.